AIP | APL Materials

Graphene-wrapped sulfur/metal organic framework-derived microporous carbon composite for lithium sulfur batteries

Renjie Chen, Teng Zhao, Tian Tian, Shuai Cao, Paul R. Coxon, Kai Xi, David Fairen-Jimenez, R. Vasant Kumar, and Anthony K. Cheetham

Citation: APL Mater. **2**, 124109 (2014); doi: 10.1063/1.4901751
View online: http://dx.doi.org/10.1063/1.4901751
View Table of Contents: http://scitation.aip.org/content/aip/journal/aplmater/2/12?ver=pdfcov
Published by the AIP Publishing

APL MATERIALS **2**, 124109 (2014)

Graphene-wrapped sulfur/metal organic framework-derived microporous carbon composite for lithium sulfur batteries

Renjie Chen,[1,2,a,b] Teng Zhao,[1,2,a] Tian Tian,[3] Shuai Cao,[2] Paul R. Coxon,[2] Kai Xi,[2,b] David Fairen-Jimenez,[3] R. Vasant Kumar,[2] and Anthony K. Cheetham[2]

[1]*Beijing Key Laboratory of Environmental Science and Engineering, School of Chemical Engineering and Environment, Beijing Institute of Technology, Beijing 100081, China*
[2]*Department of Materials Science and Metallurgy, University of Cambridge, Cambridge CB3 0FS, United Kingdom*
[3]*Department of Chemical Engineering and Biotechnology, University of Cambridge, Pembroke Street, Cambridge CB2 3RA, United Kingdom*

(Received 11 October 2014; accepted 31 October 2014; published online 16 December 2014)

A three-dimensional hierarchical sandwich-type graphene sheet-sulfur/carbon (GS-S/$C_{ZIF8\text{-}D}$) composite for use in a cathode for a lithium sulfur (Li-S) battery has been prepared by an ultrasonic method. The microporous carbon host was prepared by a one-step pyrolysis of Zeolitic Imidazolate Framework-8 (ZIF-8), a typical zinc-containing metal organic framework (MOF), which offers a tunable porous structure into which electro-active sulfur can be diffused. The thin graphene sheet, wrapped around the sulfur/zeolitic imidazolate framework-8 derived carbon (S/$C_{ZIF8\text{-}D}$) composite, has excellent electrical conductivity and mechanical flexibility, thus facilitating rapid electron transport and accommodating the changes in volume of the sulfur electrode. Compared with the S/$C_{ZIF8\text{-}D}$ sample, Li-S batteries with the GS-S/$C_{ZIF8\text{-}D}$ composite cathode showed enhanced capacity, improved electrochemical stability, and relatively high columbic efficiency by taking advantage of the synergistic effects of the microporous carbon from ZIF-8 and a highly interconnected graphene network. Our results demonstrate that a porous MOF-derived scaffold with a wrapped graphene conductive network structure is a potentially efficient design for a battery electrode that can meet the challenge arising from low conductivity and volume change. [http://dx.doi.org/10.1063/1.4901751]

Within the ever-growing family of lithium-based batteries, those based upon lithium-sulfur (Li-S) batteries are attracting significant commercial attention owing to their impressive theoretical specific energy densities approaching 2600 Wh kg^{-1} (by cell weight) which is considerably greater than the well established lithium-ion (Li-ion) batteries at 130–220 Wh kg^{-1}.[1] This difference stems from the reason that a Li-ion battery is typically based on a graphite anode and a cobalt oxide cathode, both of which can at best support Li in weight ratios of 1:10 and 1:25, respectively. Conversely, a Li-S battery uses a pure lithium metal anode with a 1:1 weight ratio and a sulfur cathode with a theoretical weight ratio of 1:2.3. Therefore, prototypes of Li-S batteries are already in the 150–220 Wh kg^{-1} range, which is on par with the current maximum specific energy density for Li-ion batteries.[2] In the near future, Li-S batteries are poised to attain both high gravimetric and volumetric energy densities beyond the values of 500 Wh kg^{-1} and 500 Wh l^{-1}, respectively. In addition, Li-S batteries can also achieve high power densities which hold their own against that of Ni-Cd batteries. It should be noted that a Li-S battery system is highly tolerant against overcharging and does not suffer from memory effect. These results provide a great impetus to spur on further research.

[a]R. Chen and T. Zhao contributed equally to this work.
[b]Authors to whom correspondence should be addressed. Electronic addresses: kx210@cam.ac.uk and chenrj@bit.edu.cn

For Li-S batteries, the foremost technical issue to overcome is poor S utilization and capacity to fade with cycling. Several reasons have been discussed in the literature for relatively poor active material utilization and cycle life. The dominant view involves parasitic loss of active S owing to the high solubility of intermediate long-chain polysulfide anions in the organic solvent and the resulting shuttle effect.[3] Specifically, S is lost by dissolving in the solvent and further by shuttling away from the cathode and even more by reacting with the Li anode. The soluble components can move in both directions in different parts of cycling. The shuttle mechanism has been directly implicated as the cause for low S utilization following the initial discharge, which is exacerbated in subsequent charge-discharge cycle. Other factors associated with S chemistry, such as its poor conductivity, incomplete reduction in some solvent systems, degradation of the S cathode by random precipitation of the discharge and charge products, and volume variations arising from significant density differences between S and the solid discharge products are also the barriers to superior electrochemical performance. Theoretically, the capacity of S is 1675 mAh g^{-1} as derived from the reduction of S_8 to the most reduced state in Li_2S. It is, therefore, not surprising that any approach which can minimize these problems can produce improved S utilization and cycle life.

Optimizing porous carbon for hosting S has been demonstrated to be an efficient strategy for partially trapping polysulfide species inside the cathode and thus minimizing problems related to shuttling. Reports in the literature have proposed various innovative porous carbon designs,[4–7] most of which mainly depend on the following principles: (a) trapping of polysulfide intermediate products by adsorption in the porous structure to prevent loss of active material and maintain cycling stability; (b) ensuring sufficient space for accommodating volume expansion during reactions; and (c) large conductive surface area for electrochemical reactions and also allowing for deposition of insoluble products. Recently, considerable research focused on introducing S into microporous carbon, which provides relatively large pore volume for hosting S and for strong confinement of polysulfides by the limited pore size. Interestingly, when pore size is tuned to less 0.5 nm, only chain-like molecular S could stably exist.[6,8] Theoretically, it avoids the formation of soluble long-chain polysulfides and thus provides a direct way to address the shuttle problem. Another potential choice of matrix for S housing is micro/mesoporous carbons derived from carbonizing metal-organic frameworks (MOFs),[7,9] which has a variety of applications[10] due to improved conductivity and inherently large surface area. MOFs, as crystalline structures, comprising metal clusters or ions coordinated to organic ligands in the form of highly porous spatial networks can provide excellent templates for preparing nanoporous carbons.[7,10] High temperature pyrolysis in inert atmospheres (~900 °C) produces a porous carbon network structure. Previously, we worked on how pore volume and pore size distribution of MOF-derived carbon loaded with sulfur influences the electrochemical performance of the cathode in a Li-S battery.[7] Tailored nanoporous carbon with high micropore (pore size <2 nm) volume loaded with S provide cathode materials with better cycle stability, while carbons with high mesopore (pore size of 2–50 nm) volume lead to improved initial discharge capacity.[7] The enhanced cycle stability can be mainly attributed to micropores, which helps to increase cycle performance by effectively restraining polysulfide anion diffusion in the organic electrolyte. However, the capacity of MOF-derived microporous carbons is relatively low due to the fact that the sulfur/carbon composites have several interfaces and grain boundaries, leading to several amorphous and irregularly connected carbon networks. Therefore, the internal resistance of the sulfur cathode is high as these interfaces act as scattering centres for electron transport. Recently, graphene, a one-atom thick carbon layer with high electrical conductivity, excellent mechanical flexibility, and large theoretical surface area, has been used in combination with S to form cathodes for Li–S batteries.[5,11–13] For example, Yang *et al.* uniformly deposited S on graphene substrate by a facile solution method, involving the simultaneous oxidation of sulfide and the reduction of GO. The prepared S/rGO composite cathode maintained a capacity of 804 mAh/g after 80 cycles.[14] In addition, graphene based hybrid S-containing cathode also exhibited much improved cycle life and rate performance.[5,11,12,15] Essentially, graphene can act as a "bridge" to form inter-connected networks and thus reducing the internal resistances from each component. Hence, hybridization of graphene and MOF-derived microporous carbons could be a promising method to further improve electrochemical performance of Li-S batteries.

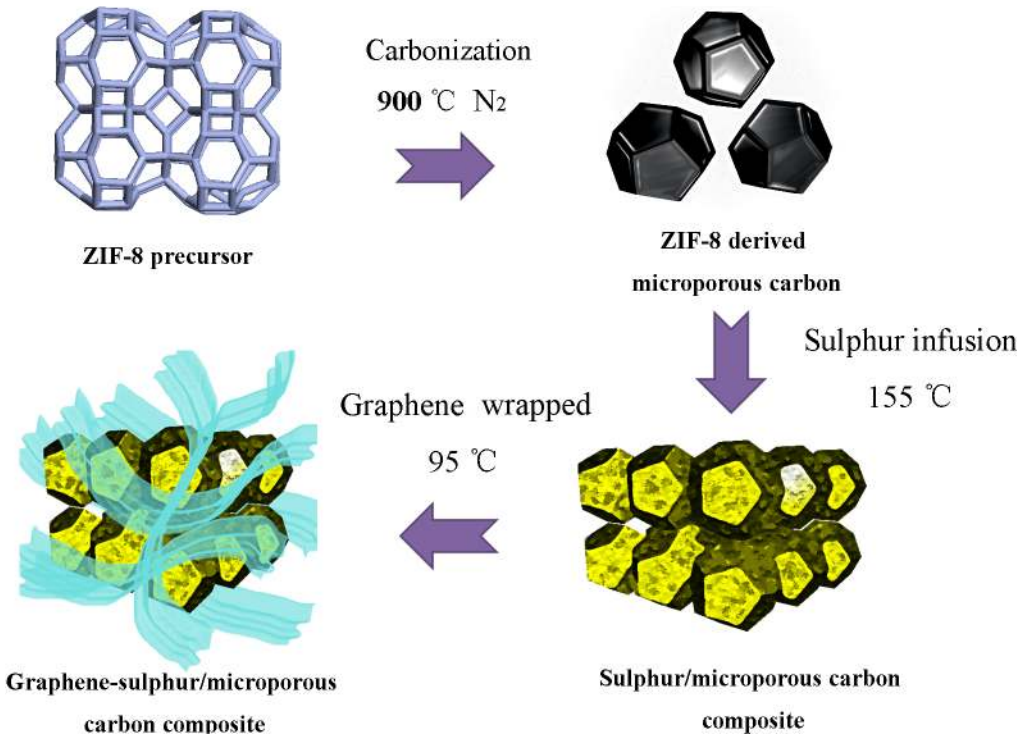

FIG. 1. Schematic illustration of the preparation of 3D hierarchically structured GS-S/$C_{ZIF8\text{-}D}$ composite.

In this work, a 3D hierarchical sandwich-type graphene sheet-sulfur/zeolitic imidazolate framework-8 derived carbon (GS-S/$C_{ZIF8\text{-}D}$) composite was synthesized by an ultrasonic method to form a Li–S battery cathode system, as shown in Fig. 1. Zeolitic Imidazolate Framework-8 (ZIF-8) is a prototypical sodalite zeolitic MOF, prepared *via* the self-assembly of Zn^{2+} and organic 2-methylimidazolate linkers, that presents large cavities (14 Å) interconnected by flexible windows[16] of about 3.4 Å. The ZIF-8 derived carbon host provides a microporous structure for housing S, while the wrapped graphene sheet (GS) effectively enhances the conductivity of the cathode while providing the ability to accommodate any volume variations during discharge-charge cycling. We have demonstrated that both good discharge capacity and cycling stability were achieved by introducing graphene to the carbonized MOFs. As a result, the Li-S battery with the GS-S/$C_{ZIF8\text{-}D}$ composite cathode was able to achieve electrochemical stability up to 120 cycles, demonstrating good electrochemical retention. The experimental details are compiled in the supplementary material.[24]

The morphology of sulfur/zeolitic imidazolate framework-8 derived carbon (S/$C_{ZIF8\text{-}D}$) and GS-S/$C_{ZIF8\text{-}D}$ composites was characterized by SEM and TEM. As illustrated in Fig. 2(a), the S/$C_{ZIF8\text{-}D}$ composites still manages to largely preserve the basic crystalline facetted shapes of the ZIF-8 precursors. Closer observation of the microporous $C_{ZIF8\text{-}D}$ particle (Fig. 2(b)) shows an average diameter of around few hundred nanometers. Fig. 2(c) is the energy dispersive X-ray spectroscopy (EDS) line scan along the diameter of the S/$C_{ZIF8\text{-}D}$ composite. The spectra indicate that S (cyan line) was uniformly distributed throughout the carbon host (red line). To examine the wrapped GS in the GS-S/$C_{ZIF8\text{-}D}$ composite, TEM observations were performed. As shown in Fig. 2(d), the thin graphene can wrap easily around the GS-S/$C_{ZIF8\text{-}D}$ owing to its flexibility. Figs. 2(e) and 2(f) show the magnified HR-TEM images of GS-S/$C_{ZIF8\text{-}D}$. The higher magnification images reveal large surface ripples and wrinkles in the GS while S is loaded into the micropores of $C_{ZIF8\text{-}D}$, which appear dark in colour arising from the higher atomic weight vis-a-vis carbon. The thickness of GS is determined to be about 5–10 layers according to the fringes. (Fig. S1 in the supplementary material).[24]

In consideration of investigating the structure of the GS-S/$C_{ZIF8\text{-}D}$ composite, XRD, Raman spectroscopy, and N_2 adsorption were conducted. Fig. 3(a) shows the XRD patterns from the individual sulfur cathode components and the as-prepared cathode itself. Although the XRD pattern

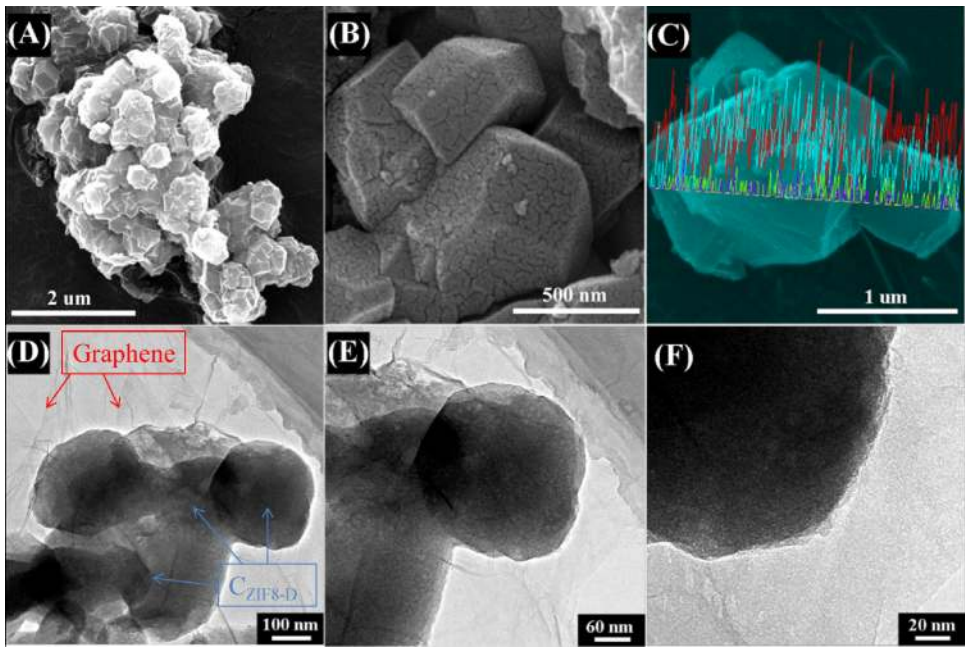

FIG. 2. (a)–(c) SEM images of the $S/C_{ZIF8\text{-}D}$ composite; (d)–(f) TEM images of the $GS\text{-}S/C_{ZIF8\text{-}D}$ composite.

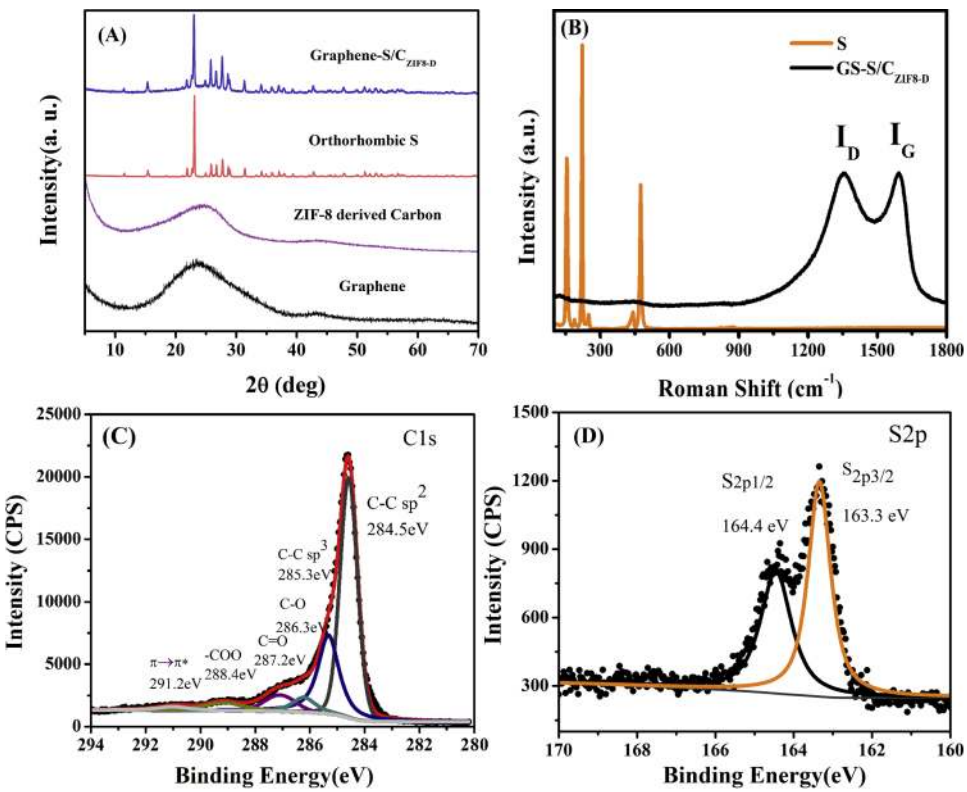

FIG. 3. (a) XRD patterns of GS, $C_{ZIF8\text{-}D}$, S, and $GS\text{-}S/C_{ZIF8\text{-}D}$ composites; (b) Raman spectra of S and $GS\text{-}S/C_{ZIF8\text{-}D}$ composites; XPS spectra of $GS\text{-}S/C_{ZIF8\text{-}D}$ composite: (c) C1S and (d) S_{2p}.

of ZIF-8 confirms its good crystallinity (Fig. S2 in the supplementary material),[24] $C_{ZIF8\text{-}D}$ only shows weak and broad peaks at $2\theta = 24°$ and 43°, almost the same as that of GS, indicating its typical amorphous structure. These broad peaks may arise from spatial correlation between elementary diffusing carbon objects and carbon atoms, and correspond to a spacing equal to $d = \lambda/(2sin\theta) = 3.7$ and 2.1 Å, respectively. These values are lower than the L_c and L_a values for graphite (3.35 and 1.42 Å, respectively), as is expected for non-graphitizable carbons.[17] On the other hand, strong sharp peaks at $2\theta = 23.0°$, 27.6°, and 26.6° in the XRD pattern of S reveal its orthorhombic crystalline structure. The characteristic peaks of each component can be observed in the XRD spectrum of the final-assembled GS-S/$C_{ZIF8\text{-}D}$ composite, confirming that no phase change has taken place during synthesis. Fig. 3(b) shows the Raman spectra of the S and GS-S/$C_{ZIF8\text{-}D}$ composite. Multiplets were observed in the S spectrum below 500 cm^{-1}, which is consistent with the crystal nature of S.[18] But such peaks cannot be detected in the same region of GS-S/$C_{ZIF8\text{-}D}$ composite spectrum, indicating that S is highly dispersed into the micropores of $C_{ZIF8\text{-}D}$ Meanwhile, two peaks observed at 1530 cm^{-1} and 1593 cm^{-1} are characteristic of the D and G bands of carbonaceous materials.[19] These signals indicate that partly graphitized carbon matrix is constructed by GS and $C_{ZIF8\text{-}D}$, which is beneficial to electron transfer from/to the insulating S and solid lithium sulfides. Fig. S3 in the supplementary material[24] shows the type I N_2 adsorption isotherm on $C_{ZIF8\text{-}D}$ obtained at 77 K, typical of a microporous material. As shown in Table S1 in the supplementary material,[24] the Brunauer–Emmett–Teller (BET) surface area was 969 m^2/g, and pore volume calculated at $P/P_0 = 0.95$ was 0.4 cm^3/g. In addition, the pore size distribution obtained through non-local density functional theory (NLDFT) shows a main peak about 6 Å, followed by two at 8 and 13 Å.[20]

To determine the chemical composition of GS-S/$C_{ZIF8\text{-}D}$ composite, X-ray photoelectron spectroscopy (XPS) elemental analysis was conducted. Fig. 3(c) shows the deconvolution of the C1s peaks. Peaks centered at 285.3 eV, 286.3 eV, 287.2 eV, and 288.4 eV are caused by the residual C–OH, C–O, C=O, and −COO, respectively.[21] Remarkably, the $\pi \rightarrow \pi^*$ shake up satellite peak at 291.2 eV is characteristic of an aromatic or conjugated system, indicating the restoration of the sp^2 hybridized carbon network. In addition, these oxygen-containing functional groups could play important roles in anchoring intermediate polysulfide ions during charge-discharge cycling. The signals of S_{2p} are weak and obscured (Fig. 3(d)), which corroborate the fact that S is mainly incorporated into the microporosity rather than on the external surfaces. Furthermore, the S_{2p} XPS spectra of the composite exhibit a doublet with peaks at 164.4 and 163.3 eV, with an intensity ratio of 1:2, which can be attributed to spin orbit coupling characteristic of $S_{2p1/2}$ and $S_{2p3/2}$.[22] These results confirm the crystalline nature of S in the composite, whose content was about 55 wt. % as determined by elemental analysis (Table S2 in the supplementary material).[24]

To understand the effect of 3D hierarchical architecture on the battery performance using the GS-S/$C_{ZIF8\text{-}D}$ composite, electrochemical characterization was conducted. Figs. 4(a) and 4(b) show the galvanostatic discharge/charge curves with GS-S/$C_{ZIF8\text{-}D}$ and S/$C_{ZIF8\text{-}D}$ composite cathodes in the 1st, 2nd, 10th, and 80th cycles at a current of 168 mA between 1.0 V and 3.0 V. The discharge curves of the two samples demonstrate three distinct potential regions. The first region is nearly a plateau at 2.4 V, then sloping down towards a second plateau at 2.1 V and a third region represented by a sudden drop to 1.8 V and then rapid decay of potential. These signatures correspond to the formation of long-chain soluble polysulfides (Li_2S_n; where n is typically 4–8) in the first region and short-chain solid sulfides (Li_2S_2 and Li_2S) in the second, and loss of redox ability in the third region. The potential hysteresis phenomenon at 1.8 V is detected, which is typically present in micropore rich cathodes.[6,8,11,23] There are two reasons that could result in such potential hysteresis phenomenon. First, this low potential reduction can be attributed to the additional polarization necessary to overcome the nano-confinement of the strong adsorption energy.[6,8,11,23] Second, the low-molecular (S_{2-4}) forms of elemental S are highly dispersed in the narrow micropores with a short chain configuration. Compared with large molecules of elemental S with crown rings, small molecules are unstable due to their high energy state (low potential difference versus metallic lithium), leading to the electrochemical reduction process starting from S_{2-4}.[8,11] Furthermore, the three plateau patterns remain the same even after 80 cycles, indicating the high cycle stability of the GS-S/$C_{ZIF8\text{-}D}$ composite.

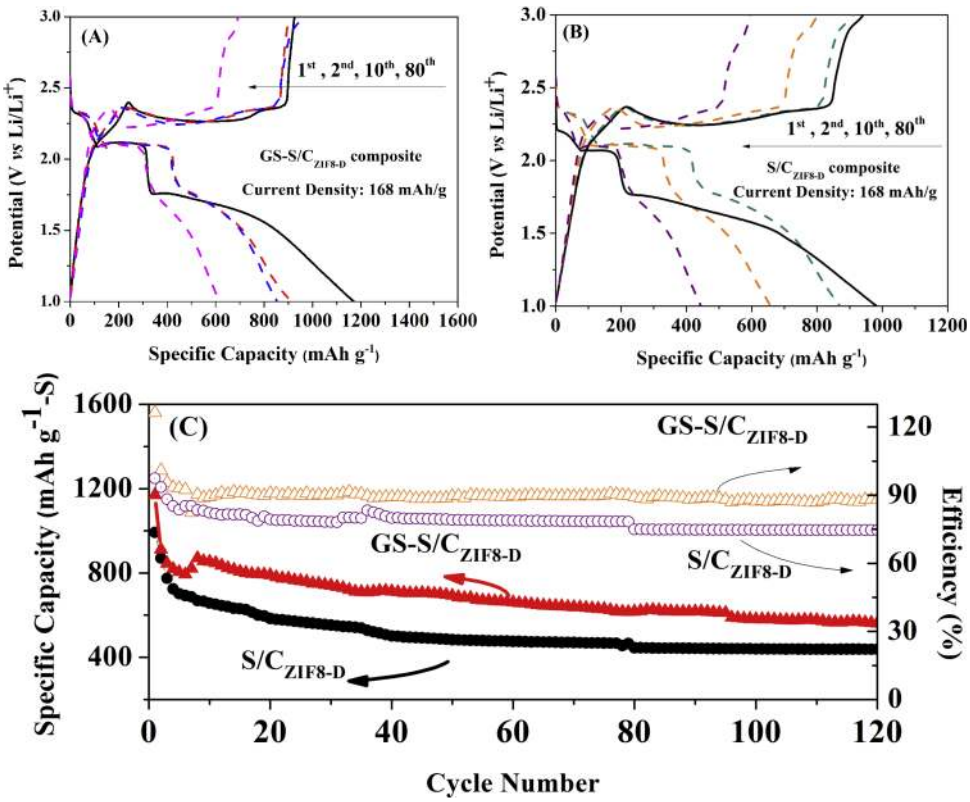

FIG. 4. Discharge/charge voltage profiles at different cycles: (a) GS-S/C_{ZIF8-D} composite; (b) S/C_{ZIF8-D} composite; (c) Cycling performance of the GS-S/C_{ZIF8-D} composite and the S/C_{ZIF8-D} composite.

Fig. 4(c) shows the cycle performance of GS-S/C_{ZIF8-D} and S/C_{ZIF8-D} composites at a current density of 168 mA g^{-1}. The GS-S/C_{ZIF8-D} composite initial discharge capacity is 1171 mAh g^{-1}, which is greater than the 982 mAh g^{-1} for the S/C_{ZIF8-D} composite. The S utilization is much improved by introducing graphene sheets in the composite. The irreversible capacity loss at the initial cycle may be because of the dissolution of residual S on the surface of C_{ZIF8-D}. After 5 cycles, deeply buried S within the micropore gradually becomes electrochemically active, resulting in improved discharge capacity. The capacity is maintained at 561 mAh g^{-1} after 120 cycles with about 48% capacity retention, while yielding an average columbic efficiency of ~90%. In contrast, both the capacity and columbic efficiency of S/C_{ZIF8-D} composite are much lower. The improved electrochemical performance of GS-S/C_{ZIF8-D} benefits from the following factors. First, the micropores in the carbon framework can encapsulate S in a highly dispersed state, achieving high usage of S; they can act as a quasi-solid-state reaction chamber where S and polysulfide ions are under solvent-deficient conditions, which can inhibit the active material loss and mitigate the shuttle effect in the liquid organic electrolyte. The results strongly indicate that, the 3D conductive network achieved by the integration of GS and C_{ZIF8-D} can help facilitate fast electron/ion transfer channels while simultaneously providing a rigid framework for confinement of volume variation during the redox reactions.

In summary, we have developed a 3D hierarchical composite cathode of GS-S/C_{ZIF8-D} for Li-S batteries. The as-prepared cathode composite demonstrates better electrochemical performance than that of the S/C_{ZIF8-D} composite. The good cycle stability can be attributed to the synergistic effect of microporous carbon from ZIF-8 and the highly conductive graphene sheet. The improved capacity is attributed to the fast charge-transfer kinetics enabled by an inter-connected graphene network with its high electrical conductivity. The results show that the composite structure of porous scaffold with conductive connection can be a promising electrode structure design for rechargeable batteries.

This work was funded by the National Science Foundation of China (21373028), National 863 Program (2011AA11A256), and the EPSRC IAA Partnership Development Award (RG/75759). D.F.-J. thanks the Royal Society for funding through a University Research Fellowship, Kai Xi thanks the Cambridge Overseas Trust, and Teng Zhao thanks the Krishnan-Ang studentships from Trinity College, Cambridge.

[1] S. Evers and L. F. Nazar, Acc. Chem. Res. **46**(5), 1135 (2012); P. G. Bruce, S. A. Freunberger, L. J. Hardwick, and J.-M. Tarascon, Nat. Mater. **11**(1), 19 (2012); Y. Yang, G. Y. Zheng, and Y. Cui, Chem. Soc. Rev. **42**(7), 3018 (2013); A. Manthiram, Y. Fu, and Y.-S. Su, Acc. Chem. Res. **46**(5), 1125 (2013); R. D. Rauh, K. M. Abraham, G. F. Pearson, J. K. Surprenant, and S. B. Brummer, J. Electrochem. Soc. **126**(4), 523 (1979).

[2] K. E. Aifantis, S. A. Hackney, and R. V. Kumar, *High Energy Density Lithium Batteries: Materials, Engineering, Applications* (John Wiley & Sons, 2010).

[3] J. Shim, K. A. Striebel, and E. J. Cairns, J. Electrochem. Soc. **149**(10), A1321 (2002).

[4] X. Ji, K. T. Lee, and L. F. Nazar, Nat. Mater. **8**(6), 500 (2009); M.-Q. Zhao, Q. Zhang, J.-Q. Huang, G.-L. Tian, J.-Q. Nie, H.-J. Peng, and F. Wei, Nat. Commun. **5**, 3410 (2014); C. Zhang, H. B. Wu, C. Yuan, Z. Guo, and X. W. Lou, Angew. Chem., Int. Ed. **51**(38), 9592 (2012).

[5] H. L. Wang, Y. Yang, Y. Y. Liang, J. T. Robinson, Y. G. Li, A. Jackson, Y. Cui, and H. J. Dai, Nano Lett. **11**(7), 2644 (2011).

[6] B. Zhang, X. Qin, G. R. Li, and X. P. Gao, Energy Environ. Sci. **3**(10), 1531 (2010).

[7] K. Xi, S. Cao, X. Peng, C. Ducati, R. V. Kumar, and A. K. Cheetham, Chem. Commun. **49**(22), 2192 (2013).

[8] S. Xin, L. Gu, N.-H. Zhao, Y.-X. Yin, L.-J. Zhou, Y.-G. Guo, and L.-J. Wan, J. Am. Chem. Soc. **134**(45), 18510 (2012).

[9] C. N. R. Rao, A. K. Cheetham, and A. Thirumurugan, J. Phys.: Condens. Matter **20**(8), 083202 (2008).

[10] S. J. Yang, T. Kim, J. H. Im, Y. S. Kim, K. Lee, H. Jung, and C. R. Park, Chem. Mater. **24**(3), 464 (2012); S. Lim, K. Suh, Y. Kim, M. Yoon, H. Park, D. N. Dybtsev, and K. Kim, Chem. Commun. **48**(60), 7447 (2012); P. Su, L. Jiang, J. Zhao, J. Yan, C. Li, and Q. Yang, Chem. Commun. **48**(70), 8769 (2012).

[11] K. Xi, P. R. Kidambi, R. Chen, C. Gao, X. Peng, C. Ducati, S. Hofmann, and R. V. Kumar, Nanoscale **6**(11), 5746 (2014).

[12] R. Chen, T. Zhao, J. Lu, F. Wu, L. Li, J. Chen, G. Tan, Y. Ye, and K. Amine, Nano Lett. **13**(10), 4642 (2013); L. W. Ji, M. M. Rao, H. M. Zheng, L. Zhang, Y. C. Li, W. H. Duan, J. H. Guo, E. J. Cairns, and Y. G. Zhang, J. Am. Chem. Soc. **133**(46), 18522 (2011).

[13] S. Lu, Y. Cheng, X. Wu, and J. Liu, Nano Lett. **13**(6), 2485 (2013); G. Zhou, L.-C. Yin, D.-W. Wang, L. Li, S. Pei, I. R. Gentle, F. Li, and H.-M. Cheng, ACS Nano **7**(6), 5367 (2013); T. Lin, Y. Tang, Y. Wang, H. Bi, Z. Liu, F. Huang, X. Xie, and M. Jiang, Energy Environ. Sci. **6**(4), 1283 (2013); S. Evers and L. F. Nazar, Chem. Commun. **48**(9), 1233 (2012).

[14] H. Sun, G.-L. Xu, Y.-F. Xu, S.-G. Sun, X. Zhang, Y. Qiu, and S. Yang, Nano Res. **5**(10), 726 (2012).

[15] C. Tang, Q. Zhang, M.-Q. Zhao, J.-Q. Huang, X.-B. Cheng, G.-L. Tian, H.-J. Peng, and F. Wei, Adv. Mater. **26**(35), 6100 (2014).

[16] D. Fairen-Jimenez, R. Galvelis, A. Torrisi, A. D. Gellan, M. T. Wharmby, P. A. Wright, C. Mellot-Draznieks, and T. Duren, Dalton Trans. **41**(35), 10752 (2012); D. Fairen-Jimenez, S. A. Moggach, M. T. Wharmby, P. A. Wright, S. Parsons, and T. Düren, J. Am. Chem. Soc. **133**(23), 8900 (2011).

[17] D. Fairén-Jiménez, F. Carrasco-Marín, D. Djurado, F. Bley, F. Ehrburger-Dolle, and C. Moreno-Castilla, J. Phys. Chem. B **110**(17), 8681 (2006).

[18] A. T. Ward, J. Phys. Chem. **72**(12), 4133 (1968).

[19] A. C. Ferrari, Solid State Commun. **143**(1–2), 47 (2007).

[20] P. I. Ravikovitch, G. L. Haller, and A. V. Neimark, Adv. Colloid Interface Sci. **76–77**(0), 203 (1998).

[21] Y.-J. Wan, L.-C. Tang, L.-X. Gong, D. Yan, Y.-B. Li, L.-B. Wu, J.-X. Jiang, and G.-Q. Lai, Carbon **69**(0), 467 (2014); S. Y. Liu, J. Xie, Q. Pan, C. Y. Wu, G. S. Cao, T. J. Z. And, and X. B. Zhao, Int. J. Electrochem. Sci. **7**(1), 354 (2012); K. Spyrou, L. Kang, E. K. Diamanti, R. Y. Gengler, D. Gournis, M. Prato, and P. Rudolf, Carbon **61**(0), 313 (2013); P. Wang, T. Jiang, C. Zhu, Y. Zhai, D. Wang, and S. Dong, Nano Res. **3**(11), 794 (2010).

[22] Y. Yang, G. Yu, J. J. Cha, H. Wu, M. Vosgueritchian, Y. Yao, Z. Bao, and Y. Cui, ACS Nano **5**(11), 9187 (2011); D. Briggs, Surf. Interface Anal. **3**(4), v (1981); F. Wu, J. Chen, L. Li, T. Zhao, Z. Liu, and R. Chen, ChemSusChem **6**(8), 1438 (2013).

[23] D.-W. Wang, G. Zhou, F. Li, K.-H. Wu, G. Q. Lu, H.-M. Cheng, and I. R. Gentle, Phys. Chem. Chem. Phys. **14**(24), 8703 (2012).

[24] See the supplementary material at http://dx.doi.org/10.1063/1.4901751 for details on the sample preparation and characterization, as well as some additional TEM image, XRD pattern, N_2 adsorption-desorption isotherms, the pore size distribution, textural characteristics, and percentage composition (by weight) of the elements.